Geosci. Model Dev. Discuss., doi:10.5194/gmd-2017-40, 2017
Manuscript under review for journal Geosci. Model Dev.
Discussion started: 13 March 2017

Geoscientific Model Development Discussions
Open Access

Neodymium isotopes in the ocean model of the Community Earth System Model (CESM1.3)

Sifan Gu[1], Zhengyu Liu[1], Alexandra Jahn[2], Johannes Rempfer[3], Jiaxu Zhang[1], Fortunat Joos[3]

[1]Department of Atmospheric and Oceanic Sciences and Center for Climate Research, University of Wisconsin-Madison, Madison, 53705, USA

[2]Department for Atmospheric and Oceanic Sciences and Institute of Arctic and Alpine Research, University of Colorado Boulder, Boulder, 80309, USA

[3]Climate and Environmental Physics, Physics Institute and Oeschger Center for Climate Change Research, University of Bern, Bern, CH-3012, Switzerland

Correspondence to: Sifan Gu (sgu28@wisc.edu)

Abstract

Neodymium (Nd) isotope ratio (ε_{Nd}) is a quasi-conservative water mass tracer and has been used increasingly as paleoclimate proxy to indicate the past evolution of ocean circulation. However, there are many uncertainties in interpreting ε_{Nd} reconstructions. For the purposes of direct comparison between climate models and proxy reconstructions, we implement Nd isotopes (^{143}Nd and ^{144}Nd) in the ocean model of the Community Earth System Model (CESM). Two versions of Nd tracers are implemented: one is the "abiotic" Nd in which the particle fields are prescribed as the particle climatology generated by the marine ecosystem module of the CESM under present day forcing; the other is the "biotic" Nd that is coupled with the marine ecosystem module. Under present day climate forcing, our model is able to simulate both Nd concentrations and ε_{Nd} in good agreement with available observations. Also, Nd concentration and ε_{Nd} in our model show similar sensitivities to the total boundary source and the ratio between particle related Nd and dissolved Nd as in previous modeling study (Rempfer et al., 2011). Therefore, our Nd-enabled ocean model provides a promising tool to study past changes in ocean and climate.

1. Introduction

Radiogenic ^{143}Nd is produced by the radioactive decay of ^{147}Sm with decay half-life of 106 billion years (Lugmair, 1974). During magma formation, Nd is more likely to enter magma than Sm, therefore, continents have lower Sm/Nd or $^{143}Nd/^{144}Nd$ compared to mantle (melt residue) and the bulk of earth. The difference of $^{143}Nd/^{144}Nd$ between continents and the bulk of earth increases with the age of the continent as $^{143}Nd/^{144}Nd$ in younger continents is more similar to the mantle. Therefore, younger (older) continents have higher (lower) $^{143}Nd/^{144}Nd$, which is more radiogenic (unradiogenic) (Goldstein and Hemming, 2003). Nd isotopic ratio ($^{143}Nd/^{144}Nd$) relative to the "bulk earth" value is reported as ε_{Nd}:

$$\varepsilon_{Nd} = [(\frac{(^{143}Nd/^{144}Nd)_{sample}}{(^{143}Nd/^{144}Nd)_{bulkearth}}) - 1] \times 10^4,$$

where $(^{143}Nd/^{144}Nd)_{bulkearth}$ is 0.512638 (Jacobsen and Wasserburg, 1980). Due to the different ages of continental crust, ε_{Nd} in continental crust varies geographically (Albarède and Goldstein, 1992). The general feature consists of the two extremes, with the most unradiogenic values (minimum) in the North Atlantic (-10 to-14), the most radiogenic values (maximum) in the Pacific (-3 to -4), and intermediate values in the Indian and Southern Ocean (-7 to -10). Seawater derives its ε_{Nd} value mainly through weathering and erosion of continental crust (Piepgras et al., 1979). Therefore, different water masses form from different locations have different ε_{Nd} values. For example, ε_{Nd} of North Atlantic Deep Water (NADW) is around -13.5, whereas ε_{Nd} of Antarctic Intermediate Water (AAIW) and Antarctic Bottom Water (AABW) is around -8. In the Atlantic, ε_{Nd} covaries with salinity (von Blanckenburg, 1999) and behaves as quasi-conservative water mass mixing tracer (Goldstein and Hemming, 2003; Piepgras and Wasserburg, 1982).

Unlike quasi-conservative ε_{Nd}, Nd concentration shows a nutrient-like behavior as it increases with depth and also along the circulation pathway (Bertram and Elderfield, 1993). The decoupling of ε_{Nd} and Nd concentration, or the so-called "Nd paradox", can be explained by reversible scavenging (Bacon and Anderson, 1982; Siddall et al., 2005) in internal Nd cycling (Siddall et al., 2008).

Geoscientific Model Development Discussions Open Access EGU

ε_{Nd} has been increasingly used in paleoceanographic studies (e.g. Piotrowski et al. 2004; Gutjahr et al. 2008; Roberts et al. 2010; Piotrowski et al. 2012) because of its ability to trace different water masses. Also, biological fractionation of Nd isotopes are negligible (Goldstein and Hemming, 2003). However, our knowledge about Nd is limited for a reliable interpretation of ε_{Nd} for past ocean changes. For example, interpretation of the Atlantic ε_{Nd} reconstructions is based on the assumption of the stable north (NADW) and south (AAIW and AABW) ε_{Nd} end-members. NADW is a mixture of low ε_{Nd} water from the Labrador Sea (<-20) and high ε_{Nd} water from the Norwegian and Greenland Sea (-7 to -10). Therefore, small changes in deep water formation during the last deglaciation, which is highly uncertain (Crocket et al., 2011; Dokken and Jansen, 1999; Labeyrie et al., 1992), will result in large changes in ε_{Nd} of NADW (van de Flierdt et al., 2016). In addition, the magnitude and isotopic composition of Nd in sources, which have been suggested to be changing in the past (e.g. : Grousset et al. 1998; Harris and Mix 1999; Amakawa et al. 2000; Lézine et al. 2005; Wolff et al. 2006; Rickli et al. 2010), may also influence ε_{Nd} in seawater (Tachikawa et al., 2003). Therefore, incorporating Nd isotopes into climate models can help to improve our understanding of Nd cycling. Previous modeling efforts of Nd have made much progress (Arsouze et al., 2009; Rempfer et al., 2011; Siddall et al., 2008). Modeling studies also suggest that ε_{Nd} end-member changes are relatively small compared with ε_{Nd} changes resulted from water mass distribution (Rempfer et al., 2012a) and glacial-deglacial ε_{Nd} variations are hard to be obtained by changes in Nd sources alone (Rempfer et al., 2012b).

Currently, many uncertainties and controversies in our understanding of past ocean evolution involve the interpretation of Nd reconstructions (e.g. Huang et al., 2014; Pahnke et al., 2008; Xie et al., 2012). Therefore, it is crucial to incorporate Nd isotopes into climate models such that model simulation and proxy record can be compared directly. This direct model-data comparison will help us to better interpret the proxy records and, furthermore, understand past ocean circulation changes. This paper is the documentation of the implementation of neodymium isotopes, ^{143}Nd and ^{144}Nd, in the ocean model of the Community Earth System Model (CESM) (Hurrell et al., 2013).

The implementation of Nd isotopes in the CESM largely follows Rempfer et al., (2011), which presents the most comprehensive study of Nd modeling to date in the intermediate complexity Bern3D model (Edwards and Marsh, 2005; Müller et al., 2006), with a successful simulation of both Nd concentration and ε_{Nd} in good agreement with observations. The parameters tuned in Rempfer et al., (2011) are based on the compilation of observations up to September 2011 by Lacan et al., (2012). Nd isotopes are included in the GEOTRACES program (Mawji et al., 2014). van de Flierdt et al., (2016) complied available Nd data up to January 2016, which includes data collected by the GEOTRACES program and additionally approximately 1,000 published data points collected outside GEOTRACES. This compilation is more than double the amount of the previous data compilation by Lacan et al., (2012). Our study uses the new database to tune model parameters. Also, our Nd module is coupled with the marine ecosystem model of the CESM (eco_Nd). In addition, we also implement an abiotic Nd (abio_Nd, similar to Rempfer et al., (2011)). Using a prescribed particle flux field, the abio_Nd can be run without the marine ecosystem module and thus has a much-reduced computation cost. Most importantly, the abio_Nd can be compared with the eco_Nd to separate the effect of circulation change and biological change on Nd. These two Nd implementations will be added to the code trunk of the current ocean model of the CESM, which will make them available to other scientist and will allow them to be maintained as CESM evolves.

This paper serves as a reference for future studies using Nd isotopes in the CESM. We will describe the model and the details of the implementation of the Nd isotopes in Section 2. The experimental design of the test simulations is described in Section 3. The results of the parameter tuning process, the comparison between the simulated Nd concentrations and ε_{Nd} with observations, and the model sensitivities to two parameters are discussed in Section 4.

2. Model Description

2.1 Physical Ocean model

The implementation of Nd is based on the code of CESM, version 1.3. CESM is a state-of-art coupled model and many of the papers describing model component and analyzing results from CESM can be found in a special collection in Journal of Climate (http://journals.ametsoc.org/topic/ccsm4-cesm1). Nd is implemented in the ocean model of the CESM, which is the Parallel Ocean Program version 2 (POP2) (Danabasoglu et al., 2012). The experiments in this study are carried out using the fully active and isotope-enabled POP2 coupled to the data atmosphere, land, ice and river runoff under the normal year forcing from CORE-II data (Large and Yeager, 2008). The model has a nominal horizontal resolution of 3° and 60 vertical layers, with a 10-m resolution in the upper 200m, increasing to 250m below 3000m. The ocean-alone model at 3° resolution is used due to its low computational cost, allowing us to carry out extensive parameter test simulations. Future applications of the Nd isotopes should use the scientifically validated 1° resolution of the CESM.

2.2 Biogeochemical component

The biogeochemical variables used in the Nd isotopes implementation (particle fluxes: $CaCO_3$, opal, POC, and dust fluxes) are generated by the marine ecosystem model in the CESM (Moore et al., 2013) through the ecosystem driver (Jahn et al., 2015). Simulated annual mean particle (CaCO3, opal, and POC) fluxes leaving the euphotic zone at 105m (Fig. 1, a~c) show patterns and magnitudes similar to those in satellite observations (Fig. 7.2.5 and 9.2.2 in Sarmiento and Gruber 2006). Surface dust deposition is taken from the ecosystem module, which is prescribed monthly surface dust flux from Luo et al., (2003) (Fig. 1d). The remineralization scheme of particle is based on the ballast model of Armstrong et al., (2002). Detailed parameterizations for particle remineralization are documented in Moore et al., (2004) with temperature dependent remineralization length scales for POC and opal.

2.3. Nd isotopes implementation

The Nd isotopes (^{143}Nd and ^{144}Nd) are added as optional tracers, which can be turned on at case build time as some other passive tracers (e.g., ideal age, carbon isotopes (Jahn et al., 2015) and water isotopes (Zhang, 2016)). We implement both abio_Nd and eco_Nd, the latter of which is coupled with the marine ecosystem model and therefore requires the ecosystem model to be turned on at the same time. The only difference between abio_Nd and eco_Nd is that abio_Nd uses a set of prescribed annually averaged dust, opal, POC, and $CaCO_3$ fields that are generated from the ecosystem module offline (Fig. 1), while eco_Nd uses these fields simultaneously computed from the ecosystem module.

The Nd module is implemented following Rempfer et al., (2011). Nd has three sources: river source, dust source, and boundary source. Sedimentation of Nd is the only sink for Nd budget. ^{143}Nd and ^{144}Nd are modeled as two separate tracers. In addition to ^{143}Nd and ^{144}Nd, Nd also has other stable isotopes and the sum of ^{143}Nd and ^{144}Nd accounts for 36% of total Nd (Magill et al., 2006). Since we use 36% of the total Nd fluxes as fluxes for ^{143}Nd and ^{144}Nd, we need to scale the simulated Nd concentration, which is the sum of ^{143}Nd and ^{144}Nd (Eq. (1)), by 1/0.36 when compared with observational Nd concentration. Fluxes for ^{143}Nd and ^{144}Nd individually are obtained by using a prescribed isotopic ratio (IR, Eq. (2)), which varies for different Nd sources as discussed below.

$$Nd = {}^{143}Nd + {}^{144}Nd \tag{1}$$

$$IR = {}^{143}Nd/{}^{144}Nd \tag{2}$$

2.3.1 Nd sources

Dust deposition over the ocean surface is one of the Nd sources to the ocean. The surface dust source, $S_{dust}(i,j)$ ($g\ m^{-3}\ s^{-1}$), is applied to the surface layer of ocean grid, and can be calculated as:

$$S_{dust}(x,y) = \frac{F_{dust}(x,y) \cdot C_{dust} \cdot \beta_{dust}}{dz_1} \tag{3}$$

Here, surface dust flux, $F_{dust}(i,j)$ ($g\ cm^{-2}\ s^{-1}$), is obtained from the ecosystem module of the CESM (Fig. 1d); global mean Nd concentration in dust is 20 μg/g (C_{dust})(Goldstein et al., 1984; Grousset et al., 1988, 1998); 2% (β_{dust}) of the total Nd in the dust is released into ocean (Greaves et al., 1994); dz_1 (m) is the thickness of the surface layer of the ocean grid. The annual total Nd from dust, f_{dust}, is 2.1×10^8 g

yr^{-1}. The individual dust sources for ^{143}Nd and ^{144}Nd can be calculated from the prescribed IR field for dust sources following Tachikawa et al., (2003) (Fig. 2c).

River runoff also provides Nd to the ocean. The river source of Nd is applied at the surface layer of the ocean. River source, $S_{river}(i,j)$ (g m^{-3} s^{-1}), can be obtained from:

$$S_{river}(x,y) = \frac{ROFF(x,y) \cdot C_{river} \cdot (1-\gamma_{river})}{dz_1} \quad (4)$$

Here, ROFF(i,j) (kg m^{-2} s^{-1}) is the river runoff from the coupler of the CESM. The simulated global annual river discharge is 41,584 km^3/yr, similar to the observational estimate of 42,439 km^3/yr in (Goldstein and Jacobsen, 1987). Nd concentration in river runoff, C_{river} (g kg^{-1}) is extrapolated from the river Nd concentration data (Goldstein and Jacobsen, 1987); we assume 70% (γ_{river}) of Nd in rivers is removed in estuaries, following Rempfer et al., (2011); dz_1 (m) is the thickness of the surface layer of ocean grid. The annual total Nd source from river runoff, f_{river}, is 1.3×10^9 g/yr, which is larger than the reported values of 5×10^8 g/yr (Goldstein and Jacobsen, 1987). The difference may be caused by the extrapolation of Nd concentration from the original data from Goldstein and Jacobsen, 1987. Individual river sources for ^{143}Nd and ^{144}Nd can be calculated from the prescribed IR field following Jeandel et al. (2007) (Fig. 2b).

Weathering of continental crust is another source of Nd. This boundary source of Nd is applied to all continental margin grids above 3,000 m (Fig. 2b). We assume a globally uniform boundary source per unit area ($f_{boundary}/A_{tot}$), where $f_{boundary}$ (g/yr) is the total boundary source and A_{tot} (m^2) is the total area of continental margin. $f_{boundary}$ is a tuning parameter, as in Rempfer et al., (2011). Boundary source used in Arsouze et al., (2009) is assumed to be exponentially decreasing with depth but observations from GEOTRACES data suggest no obvious depth dependence (van de Flierdt et al., 2016). Boundary source, $S_{boundary}(x,y,z)$ can be calculated by Eq. 5, where dz_k is the thickness of the ocean grid layers. Individual

Geosci. Model Dev. Discuss., doi:10.5194/gmd-2017-40, 2017
Manuscript under review for journal Geosci. Model Dev.
Discussion started: 13 March 2017

boundary source for ^{143}Nd and ^{144}Nd can be calculated from the prescribed IR field following Jeandel et al. (2007) (Fig. 2 b).

$$S_{boundary}(x,y,z) = \frac{f_{boundary}}{A_{tot}} \cdot \frac{1}{dz} \tag{5}$$

2.3.2 Reversible scavenging and Nd sink

Reversible scavenging is the process of Nd adsorption onto sinking particles (POC, opal, CaCO3, and dust) and desorption during particle dissolution at depth, which transports Nd downwards (Siddall et al., 2008). Total Nd can be separated into dissolved Nd phase ($[Nd]_d$) and particle associated Nd phase ($[Nd]_p$) (Eq. (6)). Particle associated Nd can be further separated into Nd associated with different particle types (POC, $CaCO_3$, opal, and dust)(Eq. (7)). At the bottom grid, Nd associated with undissolved particles is removed from the ocean through sedimentation, which is the sink for Nd budget.

$$[Nd]_t^j = [Nd]_p^j + [Nd]_d^j \tag{6}$$

$$[Nd]_p^j = [Nd]_{p,POC}^j + [Nd]_{p,CaCO_3}^j + [Nd]_{p,opal}^j + [Nd]_{p,dust}^j \tag{7}$$

The ratio of between dissolved $[Nd]_d$ and $[Nd]_p$ is given by the "equilibrium scavenging coefficient", K:

$$K_i^j = \left(\frac{[Nd]_p}{[Nd]_d}\right)^j \cdot \frac{1}{\overline{R_i}}, \tag{8}$$

where i refers to different particle types (i = POC, $CaCO_3$, opal, and dust), j refers to the different Nd isotopes (j = ^{143}Nd and ^{144}Nd), and $\frac{[Nd]_p}{[Nd]_d}$ here is another tuning parameter. $\overline{R_i}$ is the ratio between the global average particle concentration ($\overline{C_i}$, Table1) and the average density of seawater (1024.5 kg m^{-3}). We assume the dissolved Nd and the particle associated Nd are in equilibrium as in other studies (Arsouze et al., 2009; Rempfer et al., 2011; Siddall et al., 2008). Therefore, in each grid cell, the ratio between $[Nd]_p$ and $[Nd]_d$ can be obtained from Eq. (9).

Geosci. Model Dev. Discuss., doi:10.5194/gmd-2017-40, 2017
Manuscript under review for journal Geosci. Model Dev.
Discussion started: 13 March 2017

Geoscientific Model Development Discussions

$$\left(\frac{[Nd]_{p,i}(x,y,z)}{[Nd]_d(x,y,z)}\right)^j = K_i^j \cdot R_i(x,y,z) \quad , \tag{9}$$

where $R_i(x,y,z)$ is the ratio between the particle concentration, $C_i(x,y,z)$, and the density of seawater. $C_i(x,y,z)$ can be calculated from particle fluxes $F_i(x,y,z)$, which are provided by the ecosystem module, by applying a settling velocity (w) ($C_i = F_i/w$). We assume a uniform settling velocity of 1000 m yr^{-1} for all four kinds of particles. This is the velocity of the small particles, which drives the vertical cycling of isotopes (Arsouze et al., 2009; Dutay et al., 2009; Kriest, 2002). Isotopic fractionation between ^{143}Nd and ^{144}Nd during the reversible scavenging process is neglected as in Rempfer et al., (2011) because of similar molecule mass of ^{143}Nd and ^{144}Nd. We, therefore, apply the same K_i to ^{143}Nd and ^{144}Nd.

The reversible scavenging process acts as the internal cycling of Nd, which transports Nd from shallow layers to deep layers. This process can be quantified as a source term in the Nd equation

$$S_{rs}^j(x,y,z) = \frac{\partial(w \cdot [Nd]_p^j(x,y,z))}{\partial z} \quad , \tag{10}$$

where w is the settling velocity of particles (1000m yr^{-1}) and $[Nd]_p$ is Nd associated with particles, which can be calculated at every time step using Eq. (6), (7) and (9) (combined as Eq. (11)).

$$[Nd]_p^j = [Nd]_t^j \cdot \left(1 - \frac{1}{1 + K_{POC} \cdot R_{POC} + K_{CaCO_3} \cdot R_{CaCO_3} + K_{opal} \cdot R_{opal} + K_{dust} \cdot R_{dust}}\right) \tag{11}$$

Therefore, the conservation equation for Nd can be written as

$$\frac{\partial[Nd]_t^j}{\partial t} = S_{dust}^j + S_{river}^j + S_{boundary}^j + S_{rs}^j + T([Nd]_t^j) \quad , \tag{12}$$

such that the Nd concentration change is determined by three source terms in Eq. (3), (4) and (5), as well as the reversible scavenging term in Eq. (10) and the oceanic transport term (T).

3. Experiments

Geosci. Model Dev. Discuss., doi:10.5194/gmd-2017-40, 2017
Manuscript under review for journal Geosci. Model Dev.
Discussion started: 13 March 2017

Geoscientific Model Development Discussions Open Access EGU

Following Rempfer et al., (2011), our Nd model is tuned with two parameters: $f_{boundary}$ and $\frac{[Nd]_p}{[Nd]_d}$, in the abio_Nd implementation under present-day climate forcing. The tuning in the abio_Nd implementation gives us a great computational efficiency because the ecosystem module can be turned off. Yet, the parameters tuned for abio_Nd should also apply to the eco_Nd since the particle fields used in the reversible scavenging process for abio_Nd are the climatology taken from the equilibrium ecosystem module under the same climate forcing.

We have run 99 sets of experiments with different combinations of $f_{boundary}$ and $\frac{[Nd]_p}{[Nd]_d}$ to search for the optimal set of parameters that can simulate both Nd concentration and ε_{Nd} most consistent with available observations. These experiments also help us to understand the sensitivity of Nd concentration and ε_{Nd} to these two parameters. We have varied $f_{boundary}$ from 1×10^9 g yr^{-1} to 8×10^9 g yr^{-1} (more specifically, 1×10^9, 2×10^9, 3×10^9, 4×10^9, 5×10^9, 5.5×10^9, 6×10^9, 7×10^9, 8×10^9) and $\frac{[Nd]_p}{[Nd]_d}$ from 2×10^{-4} to 18×10^{-4} (more specifically, 2×10^{-4}, 4×10^{-4}, 6×10^{-4}, 8×10^{-4}, 9×10^{-4}, 10×10^{-4}, 11×10^{-4}, 12×10^{-4}, 14×10^{-4}, 16×10^{-4}, 18×10^{-4}), similar to Rempfer et al., (2011). We have not run experiments with $f_{boundary}$ equals to 0×10^9 g yr^{-1}, as experiments with low $f_{boundary}$ overall show unrealistic Nd inventory or Nd concentration.

The Nd concentrations (^{143}Nd and ^{144}Nd) are initialized from zero and each experiment is integrated for 4,000 model years (experiments with $f_{boundary} = 1\times10^9$ and 2×10^9 are initiated from 3,000 model years of the experiment with $f_{boundary} = 3\times10^9$ and then integrated for another 1,300 model years each). Nd inventory has reached equilibrium in most of the experiments at the end of the simulation. Those that do not reach equilibrium show unreasonable Nd concentrations or ε_{Nd} and drift further and further from observation as the model integrates (e.g. cases with $\frac{[Nd]_p}{[Nd]_d}<6\times10^{-4}$), and therefore are terminated at some point.

4. Results

Geosci. Model Dev. Discuss., doi:10.5194/gmd-2017-40, 2017
Manuscript under review for journal Geosci. Model Dev.
Discussion started: 13 March 2017

Geoscientific Model Development Discussions

To evaluate the performance of each parameter combination, we compare the cost function of $[Nd]_d$ and ε_{Nd} as in Rempfer et al., (2011):

$$J = \frac{1}{N}\sum_{k=1}^{N}|obs_k - model_k|, \quad (13)$$

where k represents each observational point, N is the total number of observational points, obs_k is the observational $[Nd]_d$ or ε_{Nd} and $model_k$ is the model $[Nd]_d$ or ε_{Nd} at the observational location. The cost function J measures the average deviation of the simulated $[Nd]_d$ or ε_{Nd} from observation. In addition to the cost function, we also examine the distributions of $[Nd]_d$ and ε_{Nd} compared with observations.

4.1 Cost function minimum cases

We first study the dependence of the cost function $J_{[Nd]d}$ on $f_{boundary}$ and $\frac{[Nd]_p}{[Nd]_d}$ (Fig. 3, solid line contours). Given a fixed $f_{boundary}$, for an increase in $\frac{[Nd]_p}{[Nd]_d}$, $J_{[Nd]d}$ first decreases and then increases, similar to in Rempfer et al. (2011); given a fixed $\frac{[Nd]_p}{[Nd]_d}$, for an increase in $f_{boundary}$, $J_{[Nd]d}$ also first decreases and then increases. As such, $J_{[Nd]d}$ reaches the minimum at $f_{boundary} = 2\times10^9$ g yr^{-1} and $\frac{[Nd]_p}{[Nd]_d} = 6\times10^{-4}$, which is marked by the pink square in Fig. 3. This pair of parameters of optimal $J_{[Nd]d}$ produces a $[Nd]_d$ pattern in reasonable agreement with the observation, as shown in a transect across the Atlantic and the Pacific in Fig. 4a (the transect is indicated in Fig. 2a). With this set of parameters, 79% of the $[Nd]_d$ observations are modeled within ±10 pmol kg^{-1} of the observational value. The global Nd inventory (Fig. 3, dash contours) is 4.6×10^{12} g, which is close to the current estimate of 4.2×10^{12} g (Arsouze et al., 2009; Tachikawa et al., 2003). In this set-up, model ε_{Nd} is also similar to the observations (Fig. 4b) and 76% of the points are within ±3 ε_{Nd} unit of the observational value. However, the interbasin gradient of ε_{Nd} is slightly smaller than observation (Fig. 4b). The Nd residence time (τ_{Nd}) in this setup is 1150 yr.

We then examine the dependence of $J\varepsilon_{Nd}$ on the two parameters in our model (Fig. 3, color shading). $J\varepsilon_{Nd}$ is more dominated by the change of $\frac{[Nd]_p}{[Nd]_d}$ than $f_{boundary}$,

Geosci. Model Dev. Discuss., doi:10.5194/gmd-2017-40, 2017
Manuscript under review for journal Geosci. Model Dev.
Discussion started: 13 March 2017

Geoscientific Model Development Discussions Open Access EGU

again similar to in Rempfer et al., (2011). $J\varepsilon_{Nd}$ reaches the minimum at $f_{boundary}$ = 1×10^9 g yr^{-1} and $\frac{[Nd]_p}{[Nd]_d}$ = 16×10^{-4}, which is indicated by the red triangle in Fig. 3. In this setup of optimal $J\varepsilon_{Nd}$, ε_{Nd} in the model shows a good agreement with the observation (Fig. 4d, Fig. 6e~h), with 90% of the points simulated within ±3 ε_{Nd} unit of the observational value. The residence time τ_{Nd} is now 351 yr, much shorter than that in the optimal $J_{[Nd]d}$. Therefore, the interbasin gradient of ε_{Nd} is more prominent than that in the optimal $J_{[Nd]d}$ (Fig. 4 b and d). However, $[Nd]_d$ in this setup is much smaller than the observations (Fig. 4c) and the model only simulates 19% of the points within ±10 pmol kg^{-1} of the observational Nd concentration. The Nd inventory is only 0.9×10^{12} g, much smaller than the estimate of 4.2×10^{12} g (Arsouze et al., 2009; Tachikawa et al., 2003).

As pointed out by Rempfer et al., (2011), it is not possible to have a setup of $f_{boundary}$ and $\frac{[Nd]_p}{[Nd]_d}$ that can minimize both $J_{[Nd]d}$ and $J\varepsilon_{Nd}$ simultaneously. In our model, when $J_{[Nd]d}$ reaches the minimum, the overall performance of ε_{Nd} is not good enough and when $J\varepsilon_{Nd}$ reaches the minimum, $[Nd]_d$ is too far away from the observations. Therefore, we further examined the distributions of $[Nd]_d$ and ε_{Nd} as well as the cost functions in other parameter settings as we did for the two cases with minimum $J_{[Nd]d}$ or $J\varepsilon_{Nd}$. We first pick the combinations that can produce both reasonable $[Nd]_d$ and ε_{Nd} distributions. Then we pick the one simulation that have relative better performance in simulating both $[Nd]_d$ and ε_{Nd} among those combinations, as our control experiment (CTRL). The simulation is not very sensitive to the parameter combination around CTRL, for example, if we increase $f_{boundary}$ by 1×10^9 g yr^{-1} (EXP1) or decrease $\frac{[Nd]_p}{[Nd]_d}$ by 1×10^{-4} (EXP2) from CTRL, we get similar results as CTRL (Table 2). The detailed results of CTRL are shown in the next section.

4.2 CTRL

In CTRL, $f_{bounday}$ is 4×10^9 g yr^{-1} and $\frac{[Nd]_p}{[Nd]_d}$ is 9×10^{-4} (indicated by the yellow star in Fig. 3). The total Nd inventory is 4.3×10^{12} g, which is comparable to the estimate of 4.2×10^{12} g from Arsouze et al., (2009) and Tachikawa et al., (2003).

CTRL can simulate 72% of the $[Nd]_d$ within ±10 pmol kg^{-1} of the observational value and 82% of the ε_{Nd} within ±3 ε_{Nd} unit of the observational value. The performance of simulated $[Nd]_d$ in CTRL is comparable with the optimal $J_{[Nd]d}$ case but with a much improved simulation of ε_{Nd} (Table2). The τ_{Nd} in CTRL is 785 yr, which is also within the range of available estimations (Siddall et al., 2008; Tachikawa et al., 2003).

Our CTRL can simulate the distributions of $[Nd]_d$ and ε_{Nd} in good agreement with the observations. The global and each basin distributions of $[Nd]_d$ and ε_{Nd} in CTRL are overall similar to the observations (Fig. 5-7). The correlation between model $[Nd]_d$ and observation is 0.50 and the correlation between model ε_{Nd} and observation is 0.83, both are significant at 0.01 significance level. However, $[Nd]_d$ in CTRL is smaller than observations at shallow depth and the largest and smallest ε_{Nd} found in observations are not simulated by CTRL (Fig. 6 and 8), similar to Rempfer et al. (2011).

Seafloor maps of $[Nd]_d$ and ε_{Nd} in CTRL are consistent with observations (Fig.9 and 10). $[Nd]_d$ shows a general increase along the circulation pathway from the North Atlantic to the North Pacific, in agreement with observations, except for some localized points in the North Atlantic (Fig. 9). $[Nd]_d$ at the seafloor is near 20 pmol/kg in the North Atlantic, around 30 pmol/kg in the Southern Ocean and almost 40 pmol/kg in the North Pacific. The seafloor map of ε_{Nd} in CTRL shows an interbasin gradient as in the observation (Fig. 10). The lowest ε_{Nd} values occur in the North Atlantic (<-14); the highest ε_{Nd} values occur in the North Pacific (~0), with the intermediate ε_{Nd} values in the Indian and Southern Ocean (-7 to -10), similar to observations.

Cross-sections of $[Nd]_d$ from the North Atlantic to the North Pacific in CTRL show good agreement with observations (Fig. 5a, with the track indicated by the black line in Fig. 2a), the same as in Rempfer et al., (2011). In addition to the good agreement with observations of $[Nd]_d$ at the seafloor (Fig. 9), the simulated $[Nd]_d$ agrees with observations at other depths as well (Fig. 5a). $[Nd]_d$ increases with depth at all latitudes, as in the observations, due to the reversible scavenging by particles transport Nd isotopes downward. The vertical gradient is small in the high latitude North Atlantic because of the deep convection there. In addition, the

Geosci. Model Dev. Discuss., doi:10.5194/gmd-2017-40, 2017
Manuscript under review for journal Geosci. Model Dev.
Discussion started: 13 March 2017

Geoscientific Model Development Discussions

increase along the circulation pathway is also clear in the cross-section of $[Nd]_d$. $[Nd]_d$ increases from the surface North Atlantic to the deep Southern Ocean to the deep Pacific. A comparison of the simulation and observations in selected vertical profiles of $[Nd]_d$ also show good agreement (Fig. 9), although model $[Nd]_d$ is lower than observation at shallow depth, as pointed out previously. This phenomenon is especially obvious in the region downstream of the Sahara desert plume, probably due to the overestimation of dust scavenging ability in the model (Fig. 5a). All of these features are consistent with Rempfer et al., (2011).

Cross-sections of ε_{Nd} also agree well with observations (Fig. 5b). CTRL can simulate the ε_{Nd} signatures of different water masses: NADW is -12 to -13; AAIW and AABW are -7 to -9 and the North Pacific is larger than -4. The "zig-zag" pattern of ε_{Nd} in the Atlantic is also well simulated (Goldstein and Hemming, 2003) (Fig. 10 profile 5 and 7), showing different water masses dominate in different depth ranges, alternating from AAIW to NADW to AABW from the surface to the bottom. In the Atlantic, the simulated ε_{Nd} covaries with salinity (Fig. 11), indicating northward and southward flowing water masses. However, for the same water mass, the ε_{Nd} tongue seems to be shifted to deeper depth compared with salinity, which is attributed to the effect of scavenging by sinking particles (van de Flierdt et al., 2016; Rempfer et al., 2011). In general, our simulated ε_{Nd} captures the main features of ε_{Nd} in observation. However, compared with observation, the surface Pacific ε_{Nd} in CTRL is lower (Fig. 5b and Fig. 7c), which has also been observed in Rempfer et al., (2011). Furthermore, the vertical profile of ε_{Nd} in the North Atlantic (Fig. 10 profile 4) in CTRL is quite different from observations. The simulation shows a more uniform ε_{Nd} profile but observation shows large vertical gradients, which indicates that these regional model-data discrepancies may be caused by simplification of the Nd sources as well as the coarse resolution of the model (Rempfer et al., 2011).

Overall, our CTRL shows a simulation of both Nd concentration and ε_{Nd} consistent with observations. The $f_{bounday}$ and $\frac{[Nd]_p}{[Nd]_d}$ in CTRL are near the values used in Rempfer et al., (2011). If we use the exact $f_{bounday}$ and $\frac{[Nd]_p}{[Nd]_d}$ from Rempfer et al., (2011) (CTRL_R), we can still simulate reasonable Nd concentration and ε_{Nd} (Table

2), which suggests that the parameters tuned in Rempfer et al., (2011) can also be used in other models. Also, CTRL here is tuned based on observations from van de Flierdt et al., (2016). We have also tried using the observational data from Lacan et al., (2012) to tune the parameters as in Rempfer et al., (2011) and the results of the optimal parameter combination (CTRL_old) are shown in Table 2, which show similar performance as in Rempfer et al. (2011) (CTRL_R*), as well as CTRL, suggest the robustness of the overall range of the two parameters ($f_{bounday}$ and $\frac{[Nd]_p}{[Nd]_d}$).

We also apply the tuned parameters of $f_{bounday}$ and $\frac{[Nd]_p}{[Nd]_d}$ in abio_Nd to eco_Nd and the fields of both $[Nd]_d$ and ε_{Nd} in eco_Nd are similar to the abio_Nd. The magnitude of the difference of $[Nd]_d$ and ε_{Nd} between eco_Nd and abio_Nd is quite small compare the magnitude of $[Nd]_d$ and ε_{Nd} in CTRL (Fig. 12). Therefore, parameters tuned in abio_Nd also apply to eco_Nd.

4.3 Sensitivity to $f_{bounday}$ and $\frac{[Nd]_p}{[Nd]_d}$

In this section, we show model sensitivity to $f_{bounday}$ and $\frac{[Nd]_p}{[Nd]_d}$ by studying cases with double or half $f_{bounday}$ and $\frac{[Nd]_p}{[Nd]_d}$ from CTRL. BS05 is the half $f_{bounday}$ case and BS20 is the double $f_{bounday}$ case. PD05 is the half $\frac{[Nd]_p}{[Nd]_d}$ case (note: we don't have the exact half $\frac{[Nd]_p}{[Nd]_d}$ case with $\frac{[Nd]_p}{[Nd]_d}$ =0.00045 case, so we show $\frac{[Nd]_p}{[Nd]_d}$ = 0.0004 as the half $\frac{[Nd]_p}{[Nd]_d}$ case) and PD20 is the double $\frac{[Nd]_p}{[Nd]_d}$ case (Table 2). Here, BS05, BS20, and PD20 have reached their equilibrium while PD05 has not. Although PD05 has not reached equilibrium, it does not matter for the purpose of showing model sensitivity, which will be discussed below.

A change of $f_{bounday}$ mainly effects Nd concentration, with only modest impact on ε_{Nd}, especially in the deep ocean. In comparison with CTRL, the total number of points within ±10 pmol kg^{-1} of observational $[Nd]_d$ (J1) is much reduced in BS05 and BS20 (Table 2). The $[Nd]_d$ increase with depth and circulation pathway is still

Geosci. Model Dev. Discuss., doi:10.5194/gmd-2017-40, 2017
Manuscript under review for journal Geosci. Model Dev.
Discussion started: 13 March 2017

reproduced in both BS05 and BS20, but the vertical sections of $[Nd]_d$ along the track from the North Atlantic to the North Pacific show much decreased (increased) $[Nd]_d$ in BS05 (BS20) (Fig. 13), consistent with smaller (larger) Nd inventory in BS05 (BS20)(Table 2). If the boundary source is the only Nd source, double (half) $f_{bounday}$ will lead to a double (half) of $[Nd]_d$ everywhere. However, the difference of ε_{Nd} between BS05 or BS20 and CTRL is small (Fig. 14). The number of points within ±3 ε_{Nd} unit of observational ε_{Nd} (J_2) is comparable to CTRL in both BS05 and BS20. The pattern and magnitude of the difference between BS05 (BS20) and CTRL are similar to that in Rempfer et al. (2011). The change of ε_{Nd} in BS05 and BS20 is small because the ε_{Nd} in Nd sources are fixed at prescribed values and there is no differentiation between ^{143}Nd and ^{144}Nd during the reversible scavenging. Changing $f_{bounday}$ only changes the relative contributions of the boundary source and the surface sources (dust and river), whose influences are limited to the upper 1km (Rempfer et al., 2011). If the boundary source is the only Nd source, changing $f_{bounday}$ will not change the ε_{Nd} distribution at all, since ε_{Nd} measures the ratio between ^{143}Nd and ^{144}Nd.

A change of $\frac{[Nd]_p}{[Nd]_d}$ changes both $[Nd]_d$ and ε_{Nd} significantly (Fig. 15 and 16). $J_{[Nd]d}$ in PD05 and PD20 are much larger than that in CTRL and the percentages of $[Nd]_d$ within ±10 pmol kg^{-1} of observational $[Nd]_d$ are greatly reduced (Table 2). Increasing $\frac{[Nd]_p}{[Nd]_d}$ decreases $[Nd]_d$ as it increases the compensation of $[Nd]_p$ and, in turn, sedimentation, and vice versa (Fig. 15). Increased $\frac{[Nd]_p}{[Nd]_d}$ will also reduce the vertical gradient of $[Nd]_d$ and the gradient along the circulation pathway such that $[Nd]_d$ becomes more homogeneous. This is because a larger $\frac{[Nd]_p}{[Nd]_d}$ favors the vertical transport of Nd by particles and therefore Nd is less subject to the transport by circulation. Hence, the Nd transport by circulation is overwhelmed by vertical scavenging. In addition, in the region under the Saharan dust plume, the low $[Nd]_d$ signature in CTRL is weakened in PD05 but intensified in PD20, and the low $[Nd]_d$ signature reaches almost the ocean bottom in PD20. The ε_{Nd} also shows a large difference between PD05 or PD20 and CTRL (Fig. 16). The interbasin gradient of ε_{Nd}

Geosci. Model Dev. Discuss., doi:10.5194/gmd-2017-40, 2017
Manuscript under review for journal Geosci. Model Dev.
Discussion started: 13 March 2017

Geoscientific Model Development Discussions
Open Access

increases (decreases) with the increase (decrease) of $\frac{[Nd]_p}{[Nd]_d}$, which is consistent with the shorter (longer) residence time in PD20 (PD05) (Table 2). In PD20, the North Atlantic becomes more unradiogenic while the North Pacific becomes more radiogenic compared to CTRL (opposite in PD05), consistent with Rempfer et al., (2011). With a larger $\frac{[Nd]_p}{[Nd]_d}$, more efficient scavenging by sinking particles transports more Nd from the water column to the ocean floor locally, where it is buried as sediment. This leaves less Nd that carries the ε_{Nd} signature from its source region to be transported by the circulation, resulting in a larger interbasin ε_{Nd} gradient. In addition, the slightly deeper ε_{Nd} tongue than salinity for the same water mass mentioned previously appears more (less) prominent in PD20 (PD05) as AAIW and NADW are all shifted to slightly deeper (shallower) depth than CTRL in PD20 (PD05), another indication that this mismatch is due to the reversible scavenging (Rempfer et al., 2011). It should be noted that PD05 is not completely equilibrated yet as stated previously and if run until complete equilibrium, the difference described above will be even larger.

5. Summary

Nd isotopes have been implemented into the ocean model of the CESM as both a fully biotic (eco_Nd) and an approximate abiotic (abio_Nd) version. Extensive sensitivity experiments are performed to test the model simulation with respect to $f_{boundary}$ and $\frac{[Nd]_p}{[Nd]_d}$, which are the tuning parameters in the Nd model. With the parameters we found under present climate forcing for our CTRL, our model is able to simulate the major features of the present-day global distribution of Nd and ε_{Nd}, with reasonable agreement with the observation. However, the model $[Nd]_d$ is smaller than observations at shallow depth and the model does not simulate the extremes of ε_{Nd} that are seen in the observations. These biases are similar to the biases in the Nd implementation of Rempfer et al. (2011) in the Bern3D model. Despite these shortcomings, the simulated ε_{Nd} is a useful tracer for paleoclimate studies as simulated ε_{Nd} in CTRL captures the different ε_{Nd} signatures for different water masses in observations. Therefore, our model provides a useful tool for paleoclimate studies.

Code availability:

The Nd isotope source code of both abiotic Nd and biotic Nd for CESM1.3 is included as supplementary material here.

Acknowledgement:

We thank J. Zhu for helpful suggestions on the technical issues in module implementation. This work is supported by US NSF P2C2 projects NSF1401778 and NSF1401802, DOE DE-SC0006744 and the National Science Foundation of China No. 41630527. J. Fortunat thanks for the support by the Swiss National Science Foundation (#200020_159563). Computing resources (ark:/85065/d7wd3xhc) were provided by the Climate Simulation Laboratory at NCAR's Computational and Information Systems Laboratory, sponsored by the National Science Foundation and other agencies.

References:

Albarède, F. and Goldstein, S.: World map of Nd isotopes in sea-floor ferromanganese deposits, Geology, 20(8), 761–763, 1992.

Amakawa, H., Alibo, D. S. and Nozaki, Y.: Nd isotopic composition and REE pattern in the surface waters of the eastern Indian Ocean and its adjacent seas, Geochim. Cosmochim. Acta, 64(10), 1715–1727, doi:10.1016/S0016-7037(00)00333-1, 2000.

Armstrong, R. A., Lee, C., Hedges, J. I., Honjo, S. and Wakeham, S. G.: A new, mechanistic model for organic carbon fluxes in the ocean based on the quantitative association of POC with ballast minerals, Deep. Res. Part II Top. Stud. Oceanogr., 49(1-3), 219–236, doi:10.1016/S0967-0645(01)00101-1, 2002.

Arsouze, T., Dutay, J.-C., Lacan, F. and Jeandel, C.: Reconstructing the Nd oceanic cycle using a coupled dynamical – biogeochemical model, Biogeosciences, 6(12), 2829–2846, doi:10.5194/bg-6-2829-2009, 2009.

Geosci. Model Dev. Discuss., doi:10.5194/gmd-2017-40, 2017
Manuscript under review for journal Geosci. Model Dev.
Discussion started: 13 March 2017

Geoscientific Model Development
Discussions

Bacon, M. and Anderson, R.: Distribution of Thorium Isotopes between dissolved and particulate forms in the deep sea, J. Geophys. Res. ..., 87(1), 2045–2056, 1982.

Bertram, C. J. and Elderfield, H.: The geochemical balance of the rare earth elements and neodymium isotopes in the oceans, Geochim. Cosmochim. Acta, 57(9), 1957–1986, doi:10.1016/0016-7037(93)90087-D, 1993.

von Blanckenburg, F.: Tracing past ocean circulation?, Science, 286(5446), 1862–1863, 1999.

Crocket, K. C., Vance, D., Gutjahr, M., Foster, G. L. and Richards, D. A.: Persistent Nordic deep-water overflow to the glacial North Atlantic, Geology, 39(6), 515–518, doi:10.1130/G31677.1, 2011.

Danabasoglu, G., Bates, S. C., Briegleb, B. P., Jayne, S. R., Jochum, M., Large, W. G., Peacock, S. and Yeager, S. G.: The CCSM4 ocean component, J. Clim., 25(5), 1361–1389, doi:10.1175/JCLI-D-11-00091.1, 2012.

Dokken, T. M. and Jansen, E.: Rapid changes in the mechanism of ocean convection during the last glacial period, Nature, 401(6752), 458–461, doi:10.1038/46753, 1999.

Dutay, J.-C., Lacan, F., Roy-Barman, M. and Bopp, L.: Influence of particle size and type on 231 Pa and 230 Th simulation with a global coupled biogeochemical-ocean general circulation model: A first approach, Geochemistry, Geophys. Geosystems, 10(1), doi:10.1029/2008GC002291, 2009.

Edwards, N. R. and Marsh, R.: Uncertainties due to transport-parameter sensitivity in an efficient 3-D ocean-climate model, Clim. Dyn., 24(4), 415–433, doi:10.1007/s00382-004-0508-8, 2005.

van de Flierdt, T., Griffiths, A. M., Lambelet, M., Little, S. H., Stichel, T. and Wilson, D. J.: Neodymium in the oceans: a global database, a regional comparison and implications for palaeoceanographic research, Philos. Trans. R. Soc. A Math. Phys. Eng. Sci., 374(2081), 20150293, doi:10.1098/rsta.2015.0293, 2016.

Goldstein, S. and Hemming, S.: Long-lived isotopic tracers in oceanography, paleoceanography, and ice-sheet dynamics, Treatise on geochemistry, 6(6), 453-489, 2003.

Goldstein, S. J. and Jacobsen, S. B.: The Nd and Sr isotopic systematics of river-water dissolved material: Implications for the sources of Nd and Sr in seawater, Chem. Geol. Isot. Geosci. Sect., 66(3-4), 245–272, doi:10.1016/0168-9622(87)90045-5, 1987.

Goldstein, S. L., O'Nions, R. K. and Hamilton, P. J.: A Sm-Nd isotopic study of atmospheric dusts and particulates from major river systems, Earth Planet. Sci. Lett., 70(2), 221–236, doi:10.1016/0012-821X(84)90007-4, 1984.

Greaves, M., Statham, P. and Elderfield, H.: Rare earth element mobilization from marine atmospheric dust into seawater, Mar. Chem., 46(3), 255–260, 1994.

Grousset, F. E., Biscaye, P. E., Zindler, a., Prospero, J. and Chester, R.: Neodymium isotopes as tracers in marine sediments and aerosols: North Atlantic, Earth Planet. Sci. Lett., 87(4), 367–378, doi:10.1016/0012-821X(88)90001-5, 1988.

Grousset, F. E., Parra, M., Bory, A., Martinez, P., Bertrand, P., Shimmield, G. and Ellam, R. M.: Saharan wind regimes traced by the Sr-Nd isotopic composition of subtropical Atlantic sediments: Last Glacial Maximum vs Today, Quat. Sci. Rev., 17(4-5), 395–409, doi:10.1016/S0277-3791(97)00048-6, 1998.

Gutjahr, M., Frank, M., Stirling, C. H., Keigwin, L. D. and Halliday, a. N.: Tracing the Nd isotope evolution of North Atlantic Deep and Intermediate Waters in the western North Atlantic since the Last Glacial Maximum from Blake Ridge sediments, Earth Planet. Sci. Lett., 266(1-2), 61–77, doi:10.1016/j.epsl.2007.10.037, 2008.

Harris, S. and Mix, A.: Pleistocene Precipitation Balance in the Amazon Basin Recorded in Deep Sea Sediments, Quat. Res., 26(1999), 14–26, doi:10.1006/qres.1998.2008, 1999.

Huang, K.-F., Oppo, D. W. and Curry, W. B.: Decreased influence of Antarctic intermediate water in the tropical Atlantic during North Atlantic cold events, Earth Planet. Sci. Lett., 389, 200–208, doi:10.1016/j.epsl.2013.12.037, 2014.

Hurrell, J. W., Holland, M. M., Gent, P. R., Ghan, S., Kay, J. E., Kushner, P. J., Lamarque, J. F., Large, W. G., Lawrence, D., Lindsay, K., Lipscomb, W. H., Long, M. C., Mahowald, N., Marsh, D. R., Neale, R. B., Rasch, P., Vavrus, S., Vertenstein, M., Bader, D., Collins, W. D., Hack, J. J., Kiehl, J. and Marshall, S.: The community earth system model: A framework for collaborative research, Bull. Am. Meteorol. Soc., 94(9), 1339–1360, doi:10.1175/BAMS-D-12-00121.1, 2013.

Jacobsen, S. B. and Wasserburg, G. J.: Sm-Nd isotopic evolution of chondrites, Earth Planet. Sci. Lett., 50(1), 139–155, doi:10.1016/0012-821X(80)90125-9, 1980.

Jahn, A., Lindsay, K., Giraud, X., Gruber, N., Otto-Bliesner, B. L., Liu, Z. and Brady, E. C.: Carbon isotopes in the ocean model of the Community Earth System Model (CESM1), Geosci. Model Dev., 8(8), 2419–2434, doi:10.5194/gmd-8-2419-2015, 2015.

Jeandel, C., Arsouze, T., Lacan, F., Techine, P. and Dutay, J.: Isotopic Nd compositions and concentrations of the lithogenic inputs into the ocean: A compilation, with an emphasis on the margins, Chem. Geol., 239(1-2), 156–164, doi:10.1016/j.chemgeo.2006.11.013, 2007.

Kriest, I.: Different parameterizations of marine snow in a 1D-model and their influence on representation of marine snow, nitrogen budget and sedimentation, Deep. Res. Part I Oceanogr. Res. Pap., 49(12), 2133–2162, doi:10.1016/S0967-0637(02)00127-9, 2002.

Labeyrie, L. D., Duplessy, J., Duprat, J., Juillet-Leclerc, A., Moyes, J., Michel, E., Kallel, N. and Shackleton, N. J.: Changes in the vertical structure of the North Atlantic Ocean between glacial and modern times, Quat. Sci. Rev., 11(4), 401–413, doi:10.1016/0277-3791(92)90022-Z, 1992.

Lacan, F., Tachikawa, K. and Jeandel, C.: Neodymium isotopic composition of the oceans: A compilation of seawater data, Chem. Geol., 300-301, 177–184, doi:10.1016/j.chemgeo.2012.01.019, 2012.

Large, W. G. and Yeager, S. G.: The global climatology of an interannually varying air–sea flux data set, Clim. Dyn., 33(2-3), 341–364, doi:10.1007/s00382-008-0441-3, 2008.

Lézine, A. M., Duplessy, J. C. and Cazet, J. P.: West African monsoon variability during the last deglaciation and the Holocene: Evidence from fresh water algae, pollen and isotope data from core KW31, Gulf of Guinea, Palaeogeogr. Palaeoclimatol. Palaeoecol., 219(3-4), 225–237, doi:10.1016/j.palaeo.2004.12.027, 2005.

Lugmair, G. W.: Sm-Nd ages: a new dating method, Meteoritics, 9, 369, 1974.

Luo, C., Mahowald, N. and Corral, J.: Sensitivity study of meteorological parameters on mineral aerosol mobilization, transport, and distribution, J. Geophys. Res., 108(D15), 4447, doi:10.1029/2003JD003483, 2003.

Mawji, E., Schlitzer, R., Dodas, E. M., Abadie, C., Abouchami, W., Anderson, R. F., Baars, O., Bakker, K., Baskaran, M., Bates, N. R., Bluhm, K., Bowie, A., Bown, J., Boye, M., Boyle, E. A., Branellec, P., Bruland, K. W., Brzezinski, M. A., Bucciarelli, E., Buesseler, K., Butler, E., Cai, P., Cardinal, D., Casciotti, K., Chaves, J., Cheng, H., Chever, F., Church, T. M., Colman, A. S., Conway, T. M., Croot, P. L., Cutter, G. A., De Baar, H. J. W., De Souza, G. F., Dehairs, F., Deng, F., Dieu, H. T., Dulaquais, G., Echegoyen-Sanz, Y., Lawrence Edwards, R., Fahrbach, E., Fitzsimmons, J., Fleisher, M., Frank, M., Friedrich, J., Fripiat, F., Galer, S. J. G., Gamo, T., Solsona, E. G., Gerringa, L. J. A., Godoy, J. M., Gonzalez, S., Grossteffan, E., Hattaa, M., Hayes, C. T., Heller, M. I., Henderson, G., Huang, K. F., Jeandel, C., Jenkins, W. J., John, S., Kenna, T. C., Klunder, M., Kretschmer, S., Kumamoto, Y., Laan, P., Labatut, M., Lacan, F., Lam, P. J., Lannuzel, D., Le Moigne, F., Lechtenfeld, O. J., Lohan, M. C., Lua, Y., Masqué, P., McClain, C. R., Measures, C., Middag, R., Moffett, J., Navidad, A., Nishioka, J., Noble, A., Obata, H., Ohnemus, D. C., Owens, S., Planchon, F., Pradoux, C., Puigcorbé, V., Quaya, P., Radic, A., Rehkämper,

Geosci. Model Dev. Discuss., doi:10.5194/gmd-2017-40, 2017
Manuscript under review for journal Geosci. Model Dev.
Discussion started: 13 March 2017

M., Remenyi, T., Rijkenberg, M. J. A., Rintoul, S., Robinson, L. F., Roeske, T., Rosenberg, M., Van Der Loeff, M. R., Ryabenko, E., et al.: The GEOTRACES Intermediate Data Product 2014, Mar. Chem., 177, 1–8, doi:10.1016/j.marchem.2015.04.005, 2014.

Moore, J. K., Doney, S. C. and Lindsay, K.: Upper ocean ecosystem dynamics and iron cycling in a global three-dimensional model, Global Biogeochem. Cycles, 18(4), doi:10.1029/2004GB002220, 2004.

Moore, J. K., Lindsay, K., Doney, S. C., Long, M. C. and Misumi, K.: Marine Ecosystem Dynamics and Biogeochemical Cycling in the Community Earth System Model [CESM1(BGC)]: Comparison of the 1990s with the 2090s under the RCP4.5 and RCP8.5 Scenarios, J. Clim., 26(23), 9291–9312, doi:10.1175/JCLI-D-12-00566.1, 2013.

Müller, S. A., Joos, F., Edwards, N. R. and Stocker, T. F.: Water Mass Distribution and Ventilation Time Scales in a Cost-Efficient, Three-Dimensional Ocean Model, J. Clim., 19(21), 5479–5499, doi:10.1175/JCLI3911.1, 2006.

Pahnke, K., Goldstein, S. L. and Hemming, S. R.: Abrupt changes in Antarctic Intermediate Water circulation over the past, Nat. Geosci., 1(12), 870–874, doi:10.1038/ngeo360, 2008.

Piepgras, D. and Wasserburg, G.: Isotopic Composition of Neodymiu in Waters from the Drake Passa, Science, 217(4556), 207–214, 1982.

Piepgras, D., Wasserburg, G. and Dasch, E.: The isotopic composition of Nd in different ocean masses, Earth Planet. Sci. …, 45(2), 223–236, 1979.

Piotrowski, A. M., Galy, A., Nicholl, J. A. L., Roberts, N., Wilson, D. J., Clegg, J. A. and Yu, J.: Reconstructing deglacial North and South Atlantic deep water sourcing using foraminiferal Nd isotopes, Earth Planet. Sci. Lett., 357, 289–297, doi:10.1016/j.epsl.2012.09.036, 2012.

Piotrowski, A. M., Goldstein, S. L., Hemming, S. R. and Fairbanks, R. G.: Intensification and variability of ocean thermohaline circulation through the last deglaciation, Earth Planet. Sci. Lett., 225(1-2), 205–220, doi:10.1016/j.epsl.2004.06.002, 2004.

Rempfer, J., Stocker, T. F., Joos, F., Dutay, J.-C. and Siddall, M.: Modelling Nd-isotopes with a coarse resolution ocean circulation model: Sensitivities to model parameters and source/sink distributions, Geochim. Cosmochim. Acta, 75(20), 5927–5950, doi:10.1016/j.gca.2011.07.044, 2011.

Rempfer, J., Stocker, T. F., Joos, F. and Dutay, J.-C.: On the relationship between Nd isotopic composition and ocean overturning circulation in idealized freshwater discharge events, Paleoceanography, 27(3), doi:10.1029/2012PA002312, 2012a.

Rempfer, J., Stocker, T. F., Joos, F. and Dutay, J.-C.: Sensitivity of Nd isotopic composition in seawater to changes in Nd sources and paleoceanographic implications, J. Geophys. Res., 117(C12), C12010, doi:10.1029/2012JC008161, 2012b.

Rickli, J., Frank, M., Baker, A. R., Aciego, S., de Souza, G., Georg, R. B. and Halliday, A. N.: Hafnium and neodymium isotopes in surface waters of the eastern Atlantic Ocean: Implications for sources and inputs of trace metals to the ocean, Geochim. Cosmochim. Acta, 74(2), 540–557, doi:10.1016/j.gca.2009.10.006, 2010.

Roberts, N. L., Piotrowski, A. M., McManus, J. F. and Keigwin, L. D.: Synchronous deglacial overturning and water mass source changes., Science, 327(5961), 75–8, doi:10.1126/science.1178068, 2010.

Sarmiento, J. and Gruber, N.:Ocean Biogeochemical Dynamics, Princeton University Press, 2006.

Siddall, M., Henderson, G. M., Edwards, N. R., Frank, M., Müller, S. a., Stocker, T. F. and Joos, F.: 231Pa/230Th fractionation by ocean transport, biogenic particle flux and particle type, Earth Planet. Sci. Lett., 237(1-2), 135–155, doi:10.1016/j.epsl.2005.05.031, 2005.

Siddall, M., Khatiwala, S., van de Flierdt, T., Jones, K., Goldstein, S. L., Hemming, S. and Anderson, R. F.: Towards explaining the Nd paradox using reversible scavenging in an ocean general circulation model, Earth Planet. Sci. Lett., 274(3-4), 448–461, doi:10.1016/j.epsl.2008.07.044, 2008.

Tachikawa, K., Athias, V. and Jeandel, C.: Neodymium budget in the modern ocean and paleo-oceanographic implications, J. Geophys. Res., 108(C8), 3254, doi:10.1029/1999JC000285, 2003.

Wolff, E. W., Fischer, H., Fundel, F., Ruth, U., Twarloh, B., Littot, G. C., Mulvaney, R., Röthlisberger, R., De Angelis, M., Boutron, C. F., Hansson, M., Jonsell, U., Hutterli, M. A., Lambert, F., Kaufmann, P., Stauffer, B., Stocker, T. F., Steffensen, J. P., Bigler, M., Siggaard-Andersen, M. L., Udisti, R., Becagli, S., Castellano, E., Severi, M., Wagenbach, D., Barbante, C., Gabrielli, P. and Gaspari, V.: Southern Ocean sea-ice extent, productivity and iron flux over the past eight glacial cycles., Nature, 440(7083), 491–496, doi:10.1038/nature06271, 2006.

Xie, R. C., Marcantonio, F. and Schmidt, M. W.: Deglacial variability of Antarctic Intermediate Water penetration into the North Atlantic from authigenic neodymium isotope ratios, Paleoceanography, 27(3), doi:10.1029/2012PA002337, 2012.

Zhang, J.: Understanding the deglacial evolution of deep Atlantic water masses in an isotope-enabled ocean model., PhD dissertation, University of Wisconsin-Madison,

Geosci. Model Dev. Discuss., doi:10.5194/gmd-2017-40, 2017
Manuscript under review for journal Geosci. Model Dev.
Discussion started: 13 March 2017

Geoscientific Model Development Discussions Open Access

2016.

Geosci. Model Dev. Discuss., doi:10.5194/gmd-2017-40, 2017
Manuscript under review for journal Geosci. Model Dev.
Discussion started: 13 March 2017

Geoscientific Model Development Discussions
Open Access
EGU

Figures:

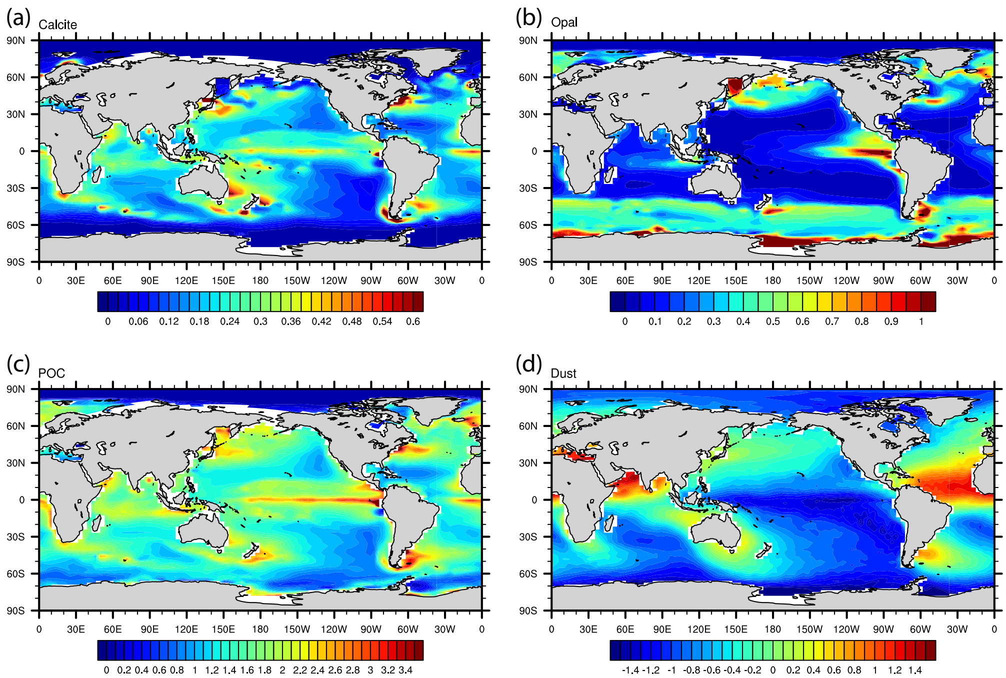

Figure 1. Annual mean particle fields produced by the ecosystem module in the CESM. (a) $CaCO_3$ flux at 105m (mol m^{-2} yr^{-1}). (b) Opal flux at 105m (mol m^{-2} yr^{-1}). (c) POC flux at 105m (mol m^{-2} yr^{-1}). (d) Log_{10} values of annual atmospheric dust deposition (g m^{-2} yr^{-1}).

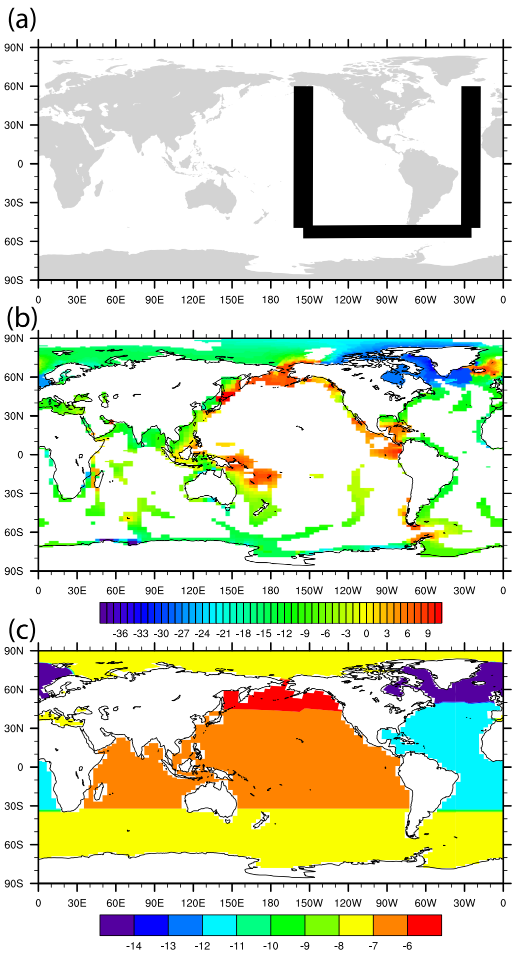

Figure 2. (a) Track of vertical sections shown in Figs. 4, 7, 13, 14, 15 and 16. (b) Global map of the continental margin in POP2 indicated by the shading. Prescribed ε_{Nd} values (Jeandel et al., 2007) for boundary source is indicated by the color. (c) Prescribed ε_{Nd} values for dust source (Tachikawa et al., 2003).

Geosci. Model Dev. Discuss., doi:10.5194/gmd-2017-40, 2017
Manuscript under review for journal Geosci. Model Dev.
Discussion started: 13 March 2017

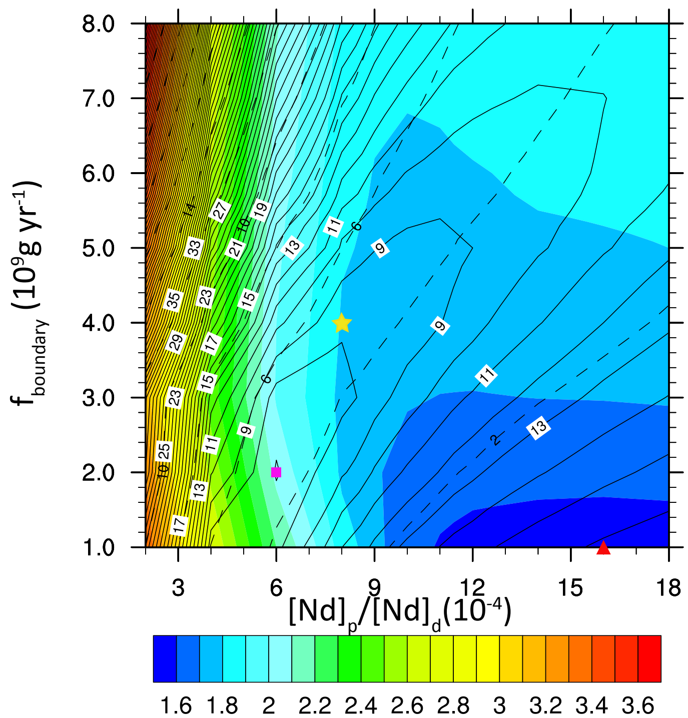

Figure 3. Contours of cost function of $[Nd]_d$ ($J_{[Nd]d}$: solid lines, unit: pmol kg^{-1}) and ε_{Nd} ($J\varepsilon_{Nd}$: color shading, unit: ε_{Nd} units) and total Nd inventory (dashed lines, unit: 10^{12}g) for different combinations of $f_{boundary}$ and $\frac{[Nd]_p}{[Nd]_d}$ at the end of each experiment. $J_{[Nd]d}$ reaching minimum is indicated by the pink square; $J\varepsilon_{Nd}$ reaching minimum is indicated by the red triangle; CTRL is indicated by the yellow star.

Particle	POC	$CaCO_3$	Opal	Dust
$\overline{C_i}$ (kg m^{-3})	2.6×10^{-6}	9.5×10^{-6}	8.3×10^{-6}	1.2×10^{-6}
$\overline{R_i}$	2.6×10^{-9}	9.3×10^{-9}	8.1×10^{-9}	1.2×10^{-9}

Tabel 1. Global average particle concentration ($\overline{C_i}$) and the dimensionless ratio $\overline{R_i}$ used for the calculation of the equilibrium scavenging coefficient (K_i) in equation 8. Our global average particle concentration of CaCO3 and opal are different from Rempfer et al. (2011) (their table 2) because we use different molecular mass

Geosci. Model Dev. Discuss., doi:10.5194/gmd-2017-40, 2017
Manuscript under review for journal Geosci. Model Dev.
Discussion started: 13 March 2017

Geoscientific Model Development Discussions
Open Access

(g/mol) to convert unit mol/m^3 to g/m^3. We use 100 g/mol for $CaCO_3$ (g-$CaCO_3$) and 60 g/mol for opal (g-SiO_2), while Rempfer et al. 2011 uses 12 g/mol for $CaCO_3$ (g-C) and 28 g/mol for opal (g-Si).

Exp	$\frac{[Nd]_p}{[Nd]_d}$	$f_{boundary}$ (g yr^{-1})	Inventory (g)	τ_{Nd} (yr)	$J_{[Nd]d}$ (pmol kg^{-1})	$J\varepsilon_{Nd}$	J_1 (%)	J_2 (%)
CTRL	0.0009	4×10^9	4.3×10^{12}	785	8.1	1.76	72	82
$J_{[Nd]d}$ min	0.0006	2×10^9	4.6×10^{12}	1282	6.9	2.07	79	76
$J\varepsilon_{Nd}$ min	0.0016	1×10^9	0.9×10^{12}	351	16.2	1.53	19	90
BS05	0.0009	2×10^9	2.8×10^{12}	796	10.1	1.71	58	83
BS20	0.0009	8×10^9	8.0×10^{12}	843	15.3	1.83	45	81
PD05	0.0004	4×10^9	9.3×10^{12}	1680	18.7	2.5	26	70
PD20	0.0018	4×10^9	2.2×10^{12}	400	14.4	1.88	42	80
CTRL_R	0.001	5.5×10^9	5.1×10^{12}	720	9.3	1.78	64	83
CTRL_R*	0.001	5.5×10^9	4.2×10^{12}	700	9	1.66	70	83
EXP1	0.0008	5×10^9	6.02×10^{12}	915	9.8	1.8	60	82
EXP2	0.0009	5×10^9	5.29×10^{12}	805	9.1	1.8	66	82
CTRL_old	0.0008	4×10^9	5.0×10^{12}	900	9.6	1.8	71	82

Table 2. Parameters and general performance for different experiments. CTRL is the parameters tuned for our model. $J_{[Nd]d}$ min and $J\varepsilon_{Nd}$ min are cost function of $[Nd]_d$ and ε_{Nd} reach minimum. Model sensitivities on $f_{boundary}$ are BS05 and BS20, where we half (BS05) or double (BS20) the $f_{boundary}$ based on CTRL. Model sensitivities on $\frac{[Nd]_p}{[Nd]_d}$ are PD05 and PD20, where we half (PD05) or double (PD20) $\frac{[Nd]_p}{[Nd]_d}$ based on CTRL. CTRL_R is the experiments using the parameters in the CTRL in Rempfer et al. (2011). CTRL_R* are the results of the CTRL in Rempfer et al., (2011). CTRL_old is the optimal parameter combination if we use the observational data from Lacan et al., (2012) as in Rempfer et al., (2011). J_1 is the percentage of the observation, which model $[Nd]_d$ is within ±10 pmol kg^{-1} of observation. J_2 is the percentage of the observation, which model ε_{Nd} is within ±3 ε_{Nd} unit of observation.

Geosci. Model Dev. Discuss., doi:10.5194/gmd-2017-40, 2017
Manuscript under review for journal Geosci. Model Dev.
Discussion started: 13 March 2017

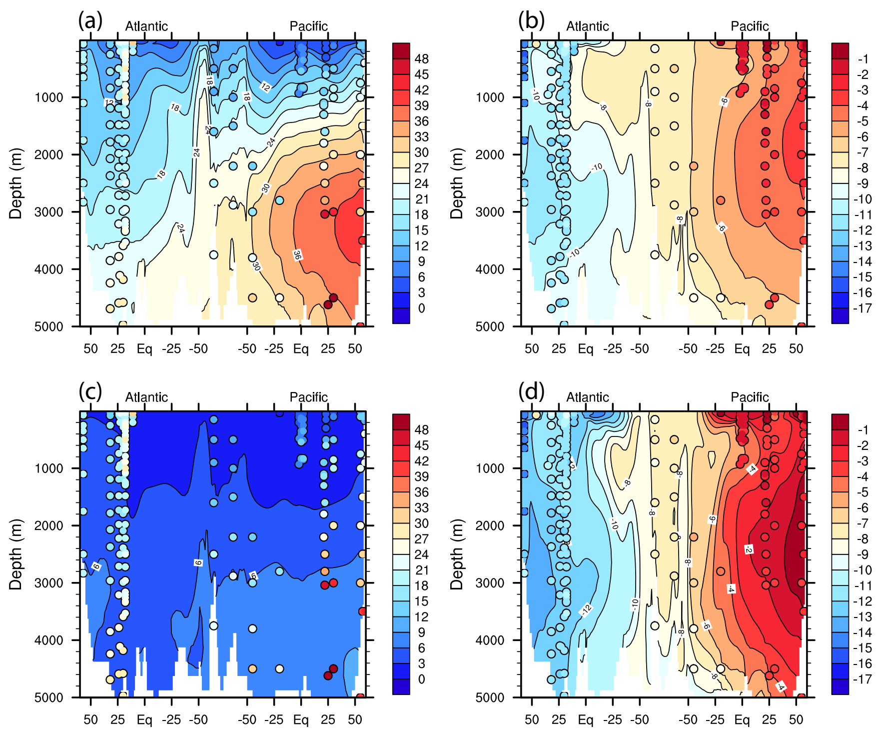

Figure 4. Vertical sections of $[Nd]_d$ (left) and ε_{Nd} (right) along a track from the North Atlantic to the North Pacific when $J_{[Nd]d}$ reaches minimum (a and b) and $J\varepsilon_{Nd}$ reaches minimum (c and d). Color contours are model results and observations are attached as filled cycles using the same color map.

Geosci. Model Dev. Discuss., doi:10.5194/gmd-2017-40, 2017
Manuscript under review for journal Geosci. Model Dev.
Discussion started: 13 March 2017

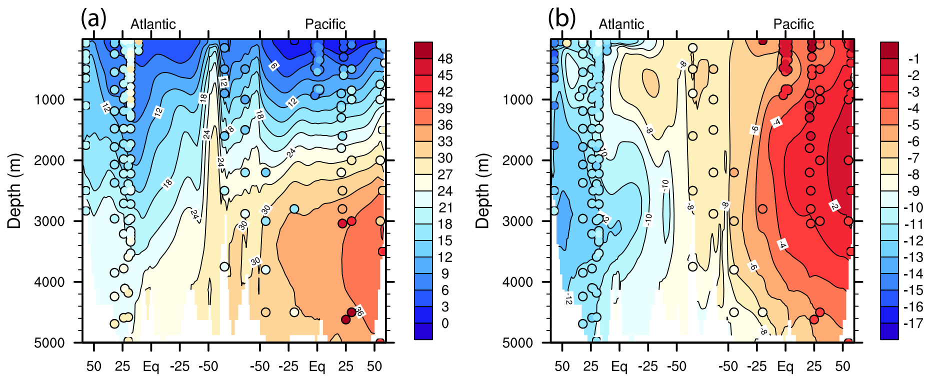

Figure 5. Vertical sections of $[Nd]_d$ (a) and ε_{Nd} (b) along the track (indicated in Fig.2 (a)) from the North Atlantic to the North Pacific in CTRL. Color contours are model results and observations are attached as filled cycles using the same color map.

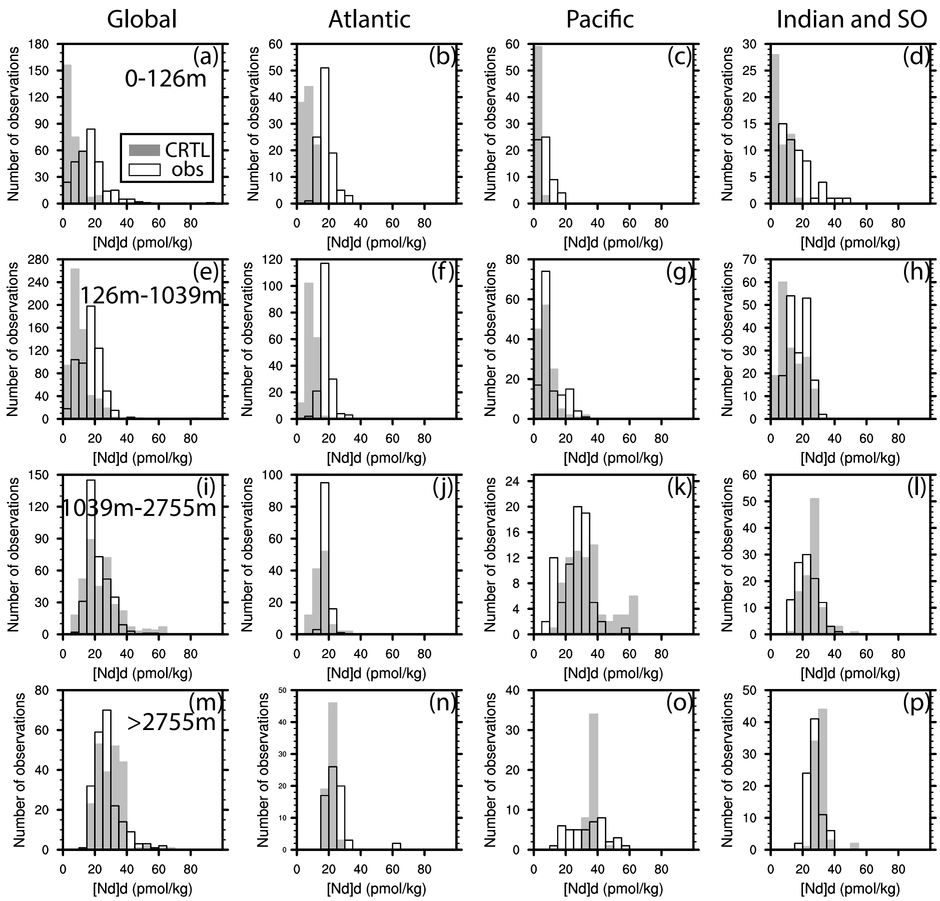

Figure 6. Histograms of observational (white) $[Nd]_d$ and model values at observation location in CTRL (grey). First column shows the distribution of the global ocean, second column for the Atlantic, third column for the Pacific and the forth column for the Indian and Southern Ocean. Each ocean basin has been separated into different depth ranges: first row for 0-126m, second row for 126m-1039m, third row for 1039m-2755m and the forth row for ocean deeper than 2755m.

Geosci. Model Dev. Discuss., doi:10.5194/gmd-2017-40, 2017
Manuscript under review for journal Geosci. Model Dev.
Discussion started: 13 March 2017

Geoscientific Model Development Discussions

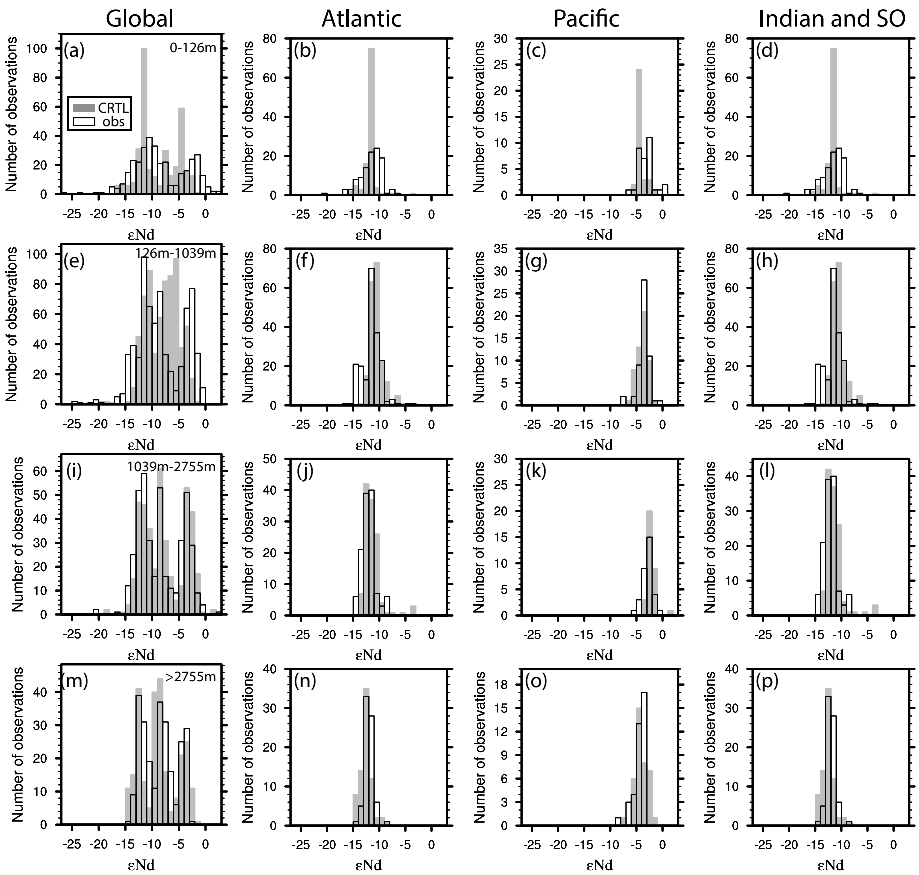

Figure 7. Histograms of observational (white) ε_{Nd} and model values at observation location in CTRL (grey). First column shows the distribution of the global ocean, second column for the Atlantic, third column for the Pacific and the forth column for the Indian and Southern Ocean. Each ocean basin has been separated into different depth ranges: first row for 0-126m, second row for 126m-1039m, third row for 1039m-2755m and the forth row for ocean deeper than 2755m.

Geosci. Model Dev. Discuss., doi:10.5194/gmd-2017-40, 2017
Manuscript under review for journal Geosci. Model Dev.
Discussion started: 13 March 2017

Geoscientific Model Development Discussions
Open Access
EGU

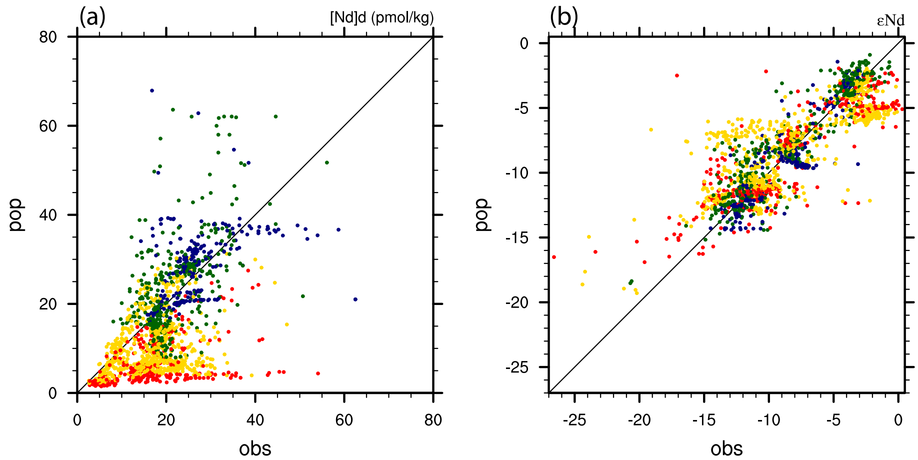

838
839 Figure 8. Scatter plot of observational $[Nd]_d$ (a) and ε_{Nd} (b) in CTRL. Colors indicated
840 different depth range: 0-126m (red), 126m-1039m (yellow), 1039m-2755m (green)
841 and deeper than 2755m (blue).

Geosci. Model Dev. Discuss., doi:10.5194/gmd-2017-40, 2017
Manuscript under review for journal Geosci. Model Dev.
Discussion started: 13 March 2017

Geoscientific Model Development Discussions

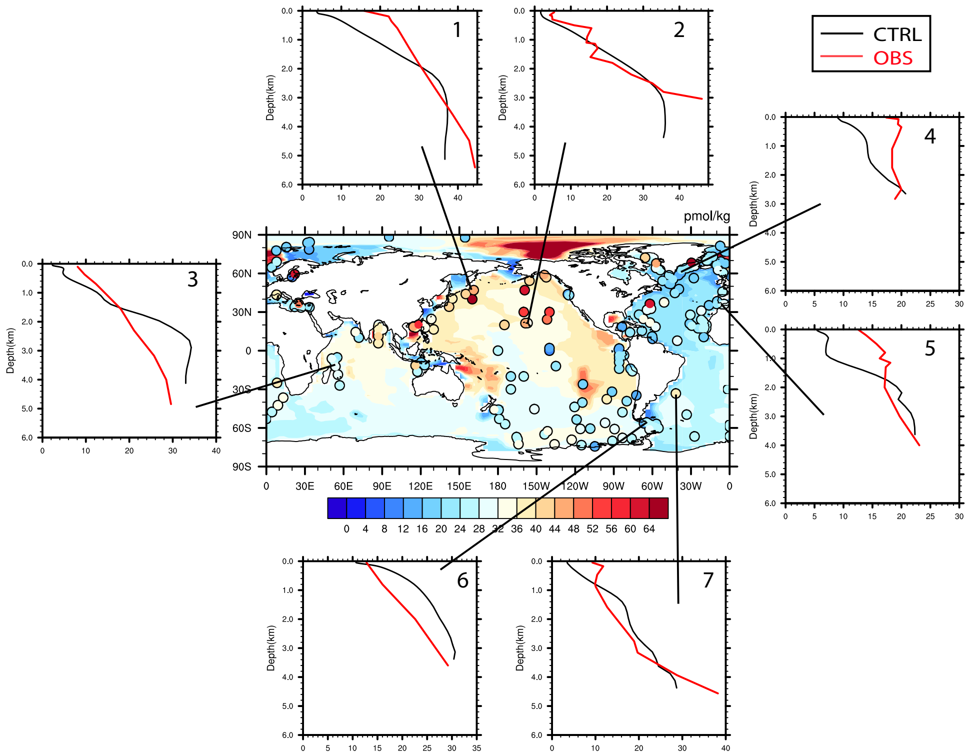

842
843
844 Figure 9. Global map of $[Nd]_d$ at the seafloor in CTRL along with selected vertical
845 profiles of $[Nd]_d$. Color contours are model results and observations are attached as
846 filled cycles using the same color map. Profiles in black are model results and
847 profiles in red are observations.
848
849
850

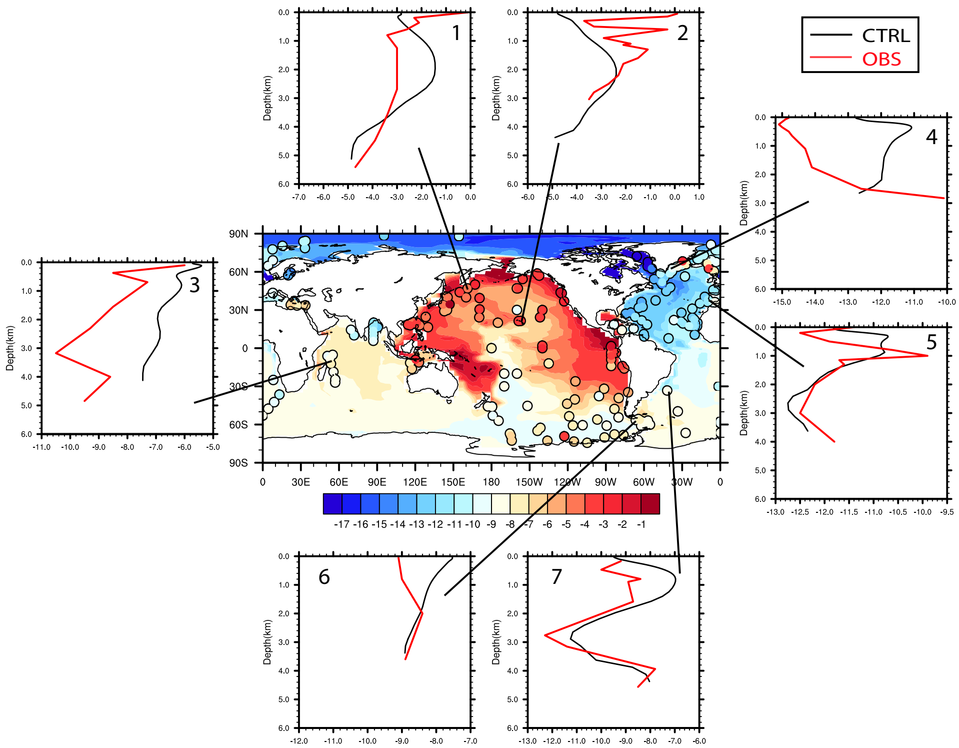

Figure 10. Global map of ε_{Nd} at the seafloor in CTRL along with selected vertical profiles of ε_{Nd}. Color contours are model results and observations are attached as filled cycles using the same color map. Profiles in black are model results and profiles in red are observations.

Geosci. Model Dev. Discuss., doi:10.5194/gmd-2017-40, 2017
Manuscript under review for journal Geosci. Model Dev.
Discussion started: 13 March 2017

Geoscientific Model Development Discussions
Open Access

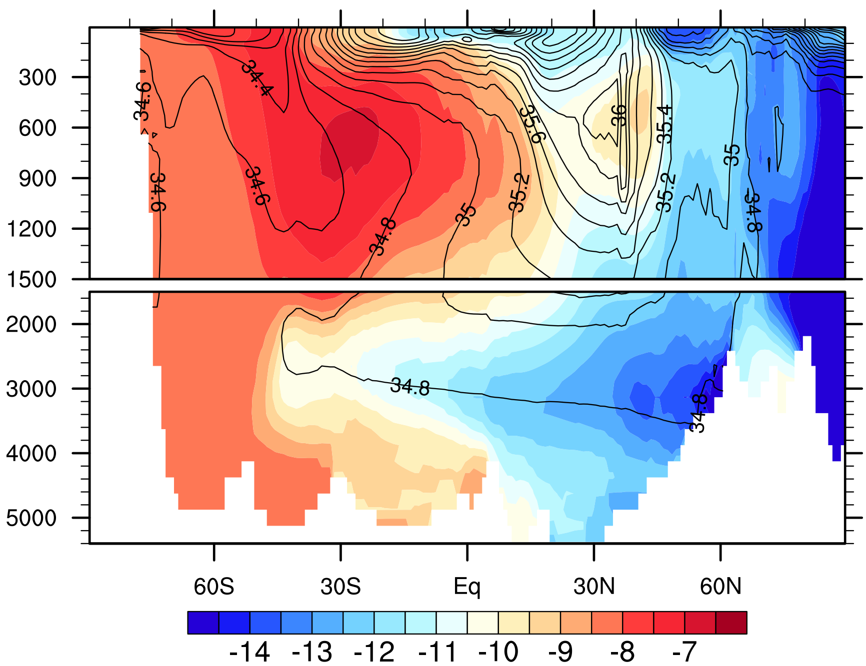

Figure 11. Zonal mean Atlantic ε_{Nd} (color) and salinity (solid line) in CTRL.

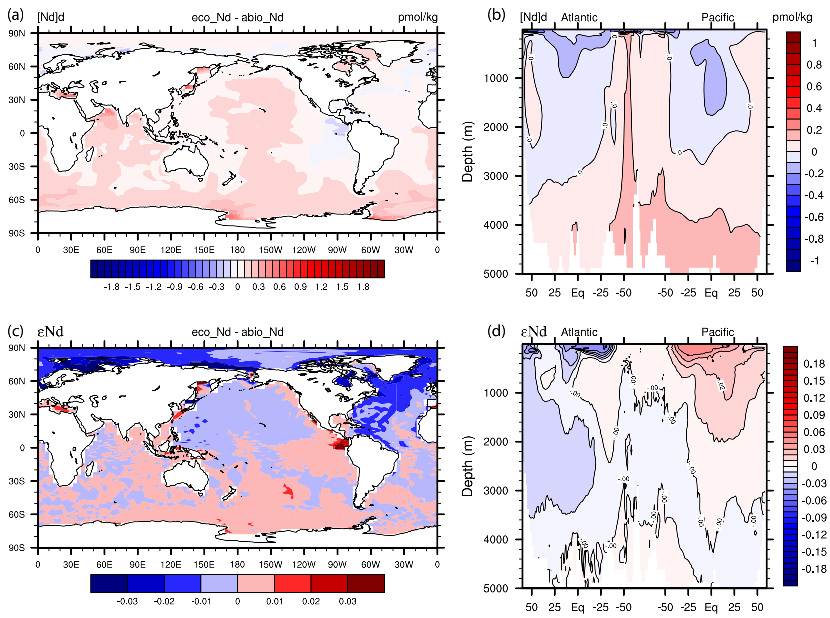

Figure 12. Difference of $[Nd]_d$ and ε_{Nd} between eco_Nd and abio_Nd. (a) $[Nd]_d$ difference at the seafloor. (b) $[Nd]_d$ difference along the track (indicated in Fig.2 (a)). (c) ε_{Nd} difference at the seafloor. (d) ε_{Nd} difference along the track.

Geosci. Model Dev. Discuss., doi:10.5194/gmd-2017-40, 2017
Manuscript under review for journal Geosci. Model Dev.
Discussion started: 13 March 2017

Geoscientific Model Development Discussions

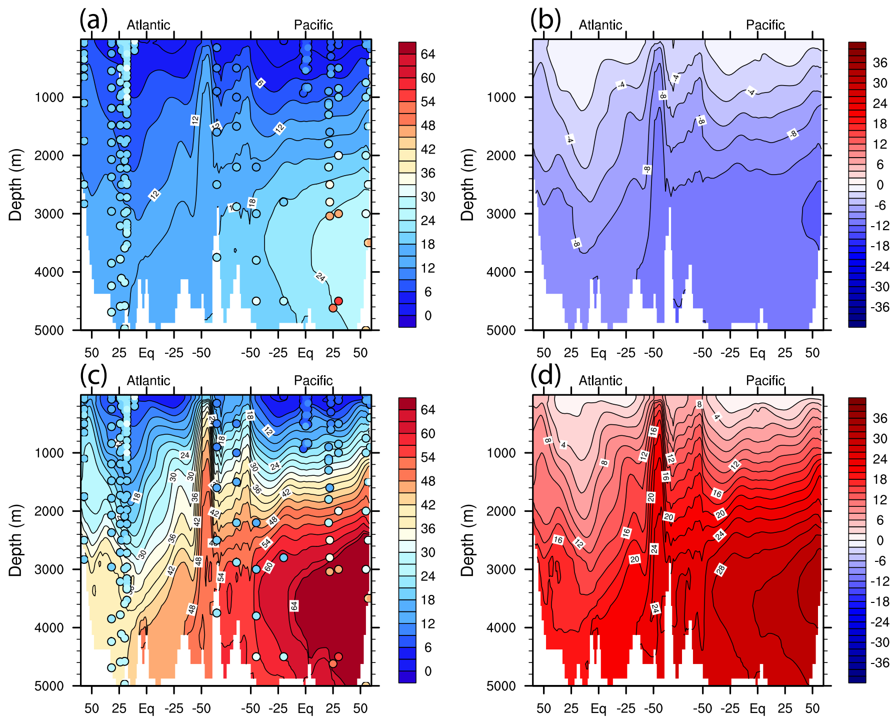

Figure 13. Vertical sections of $[Nd]_d$ along the track from the North Atlantic to the North Pacific (indicated in Fig.2 (a)) for the sensitivity on $f_{boundary}$: (a) BS05 (b) difference between BS05 and CTRL. (c) BS20 (d) difference between BS20 and CTRL. Observations are attached as filled cycles using the same color map in (a) and (c).

Geosci. Model Dev. Discuss., doi:10.5194/gmd-2017-40, 2017
Manuscript under review for journal Geosci. Model Dev.
Discussion started: 13 March 2017

Geoscientific Model Development Discussions
Open Access

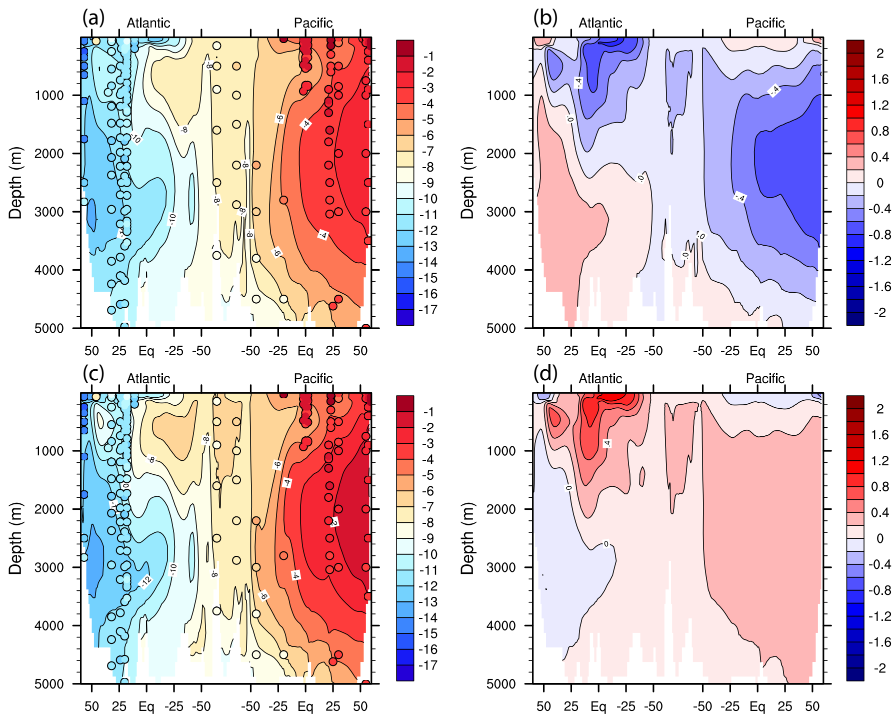

Figure 14. Vertical sections of ε_{Nd} along the track from the North Atlantic to the North Pacific (indicated in Fig.2 (a)) for the sensitivity on $f_{boundary}$: (a) BS05 (b) difference between BS05 and CTRL. (c) BS20 (d) difference between BS20 and CTRL. Observations are attached as filled cycles using the same color map in (a) and (c).

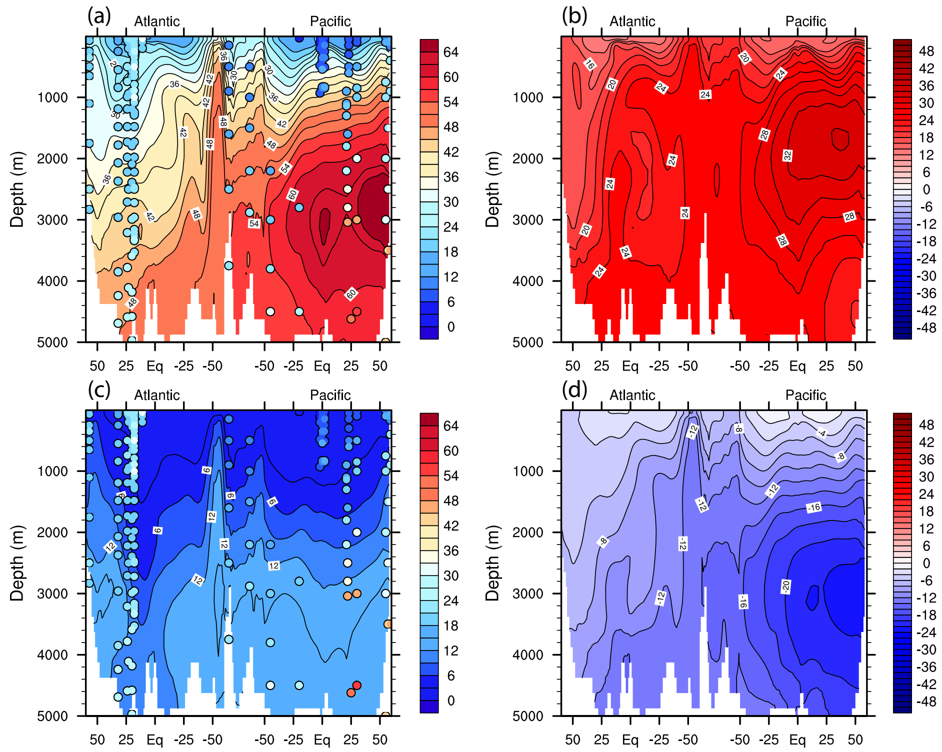

Figure 15. Vertical sections of $[Nd]_d$ along the track from the North Atlantic to the North Pacific (indicated in Fig.2 (a)) for the sensitivity on $\frac{[Nd]_p}{[Nd]_d}$: (a) PD05 (b) difference between PD05 and CTRL. (c) PD20 (d) difference between PD20 and CTRL. Observations are attached as filled cycles using the same color map in (a) and (c).

Geosci. Model Dev. Discuss., doi:10.5194/gmd-2017-40, 2017
Manuscript under review for journal Geosci. Model Dev.
Discussion started: 13 March 2017

Geoscientific Model Development Discussions

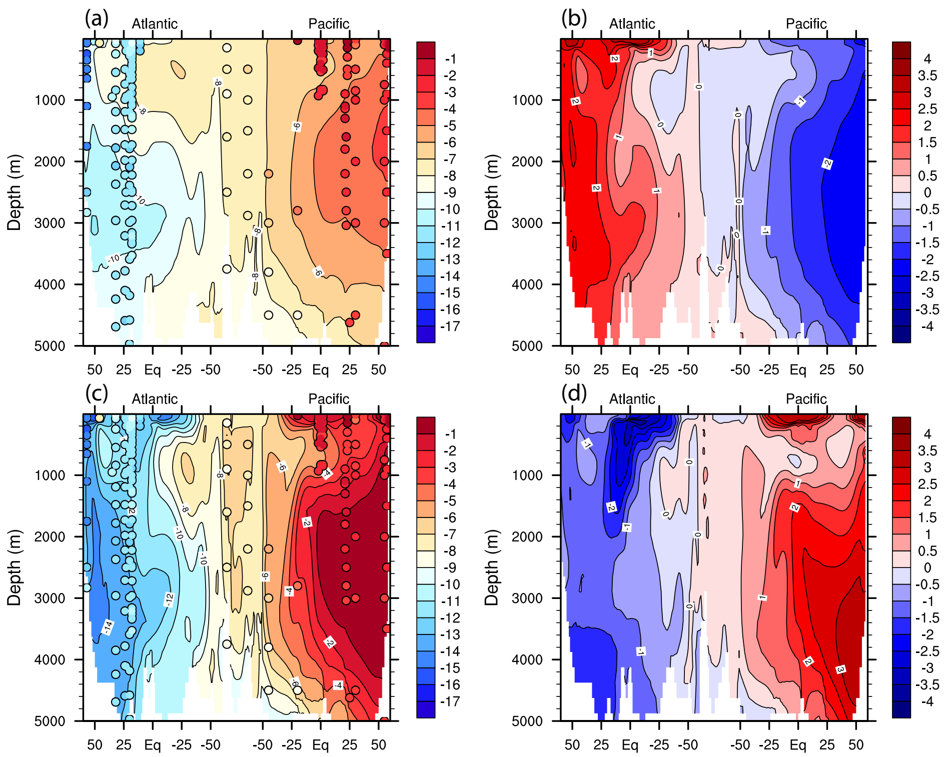

Figure 16. Vertical sections of ε_{Nd} along the track from the North Atlantic to the North Pacific (indicated in Fig.2 (a)) for the sensitivity on $\frac{[Nd]_p}{[Nd]_d}$: (a) PD05 (b) difference between PD05 and CTRL. (c) PD20 (d) difference between PD20 and CTRL. Observations are attached as filled cycles using the same color map in (a) and (c).